# INTERFEROMETRY OF THE COSMIC MICROWAVE BACKGROUND

RAFAEL REBOLO [1,2] and the VSA consortium[1,3,4]
*1 Instituto de Astrofísica de Canarias, E-38200 La Laguna, Tenerife, SPAIN*
*2 Consejo Superior de Investigaciones Científicas, SPAIN*
*3 Astrophysics Group, Cavendish Laboratory, University of Cambridge, Madingley R oad, CB3 OHE, UK*
*4 Jodrell Bank Observatory, University of Manchester, Macclesfield, Cheshire, SK 11 9DL, UK*

**Abstract:** We describe the Very Small Array (VSA) and review the recent results on the angular power spectrum of the Cosmic Microwave Background (CMB) obtained in the Ka-band ($\nu \approx 33$ GHz) with this instrument. This array has covered an $\ell$-range of 150 to 1500 with a relatively high resolution in $\ell$ compared to previous measurements at $\ell \geq 1000$; this is achieved by using mosaiced observations in 7 regions covering a total of approximately 82 sq. degrees. Our resolution of $\Delta\ell \approx 60$ between $\ell = 300$ and $\ell = 1500$ allows the first 3 acoustic peaks to be identified. Contamination by extragalactic radiosources brighter than 20 mJy has been taken into account by simultaneously monitoring identified sources with a high resolution interferometer. In addition, it has been performed a statistical correction for the small residual contribution from weaker sources that are below this flux limit. There is good agreement between the VSA power spectrum and that obtained by WMAP and other higher resolution experiments like ACBAR and CBI.

We have set constraints on cosmological parameters using VSA data and combinations with other CMB data and external priors. Within the flat $\Lambda$CDM model, the combined VSA+WMAP data without external priors gives $\Omega_{\rm b}h^2 = 0.0234^{+0.0012}_{-0.0014}$, $\Omega_{\rm dm}h^2 = 0.111^{+0.014}_{-0.016}$, $h = 0.73^{+0.09}_{-0.05}$, $n_{\rm S} = 0.97^{+0.06}_{-0.03}$, $10^{10}A_{\rm S} = 23^{+7}_{-3}$ and $\tau = 0.14^{+0.14}_{-0.07}$. We also find evidence for a running spectral index of density fluctuations, $n_{\rm run} = -0.069 \pm 0.032$ at a level of more than 95% confidence. However, inclusion of prior information from the 2dF galaxy redshift survey reduces the significance of the result. When a general cosmological model with 12 parameters is considered we find consistency with other analyses available in the literature. The evidence for $n_{\rm run} < 0$ is only marginal within this model. The fraction of dark matter in neutrinos is constrained to $f_\nu < 0.087$ (95% confidence limit) which implies that $m_\nu < 0.32$ eV if all the three neutrino species have the same mass.

# 1 Introduction

The CMB is a relic of the primitive Universe observed today as a largely isotropic radiation with Planckian spectral energy distribution of temperature $T_0$=2.726±0.004 K (95 % C.L.) [1]. It carries the imprint of the primordial density fluctuations that originated the large scale structure of the Universe providing extremely valuable information on the physical conditions of the very hot and dense early Universe. Peaks in the CMB angular power spectrum are a consequence of the evolution of pressure waves in the primordial plasma before the recombination epoch [2, 3]. These peaks provide information about the primordial density fluctuations, geometry, matter and radiation content and ionization history of the Universe. Their amplitudes and positions are sensitive to many of the most important cosmological parameters.

Following the detection of large angular scale fluctuations in the CMB temperature distribution by the Differential Microwave Radiometer on board the Cosmic Background Explorer (COBE) satellite [4], a major effort has been devoted to measure the angular power spectrum of primordial anisotropies. Several experiments have consistently detected acoustic peaks in the power spectrum in the $\ell$-range $100 - 1000$ [5, 6, 7, 8, 9, 10] and a fall-off in power at high-$\ell$ from the damping tail [11, 12, 13]. The Wilkinson Microwave Anisotropy Probe, henceforth $WMAP$, has provided the highest sensitivity measurements [14, 15] over the $\ell$-range $2-700$. The resulting power spectrum is cosmic variance limited up to $\ell = 350$ and delineates the first 2 peaks (at $\ell \sim 220$ and 550) with excellent signal-to-noise. These recent CMB measurements have brought impressive detailed cosmological information on a wide range of parameters [16], but $WMAP$ is limited in angular resolution and hence has not measured the power spectrum above $\ell \sim 800$ with good signal-to-noise. Additional observations at high angular resolution (angular scales and multipoles are related according to the expression $\theta \sim \frac{120^\circ}{\ell}$) are still required to break some of the degeneracies inherent in the CMB power spectrum. Here, we review the recent measurements obtained by VSA out to a multipole of $\ell = 1500$ [17] and discuss their cosmological implications.

# 2 Interferometry and basic CMB formalism

The temperature fluctuations of the CMB on the sky $\frac{\Delta T}{T_0}(\vec{n}) \equiv \frac{T(\vec{n})-T_0}{T_0}$ are usually expressed in terms of an expansion into spherical harmonics

$$\frac{\Delta T}{T_0}(\vec{n}) = \sum_{\ell=1}^{\infty} \sum_{m=-\ell}^{\ell} a_{\ell m} Y_{\ell m}(\vec{n}) \qquad (1)$$

where $\vec{n}$ is a unity vector that indicates the line of sight. Most of the models predict the temperature field to be gaussian. In that case, the statistical properties are

completely characterized by the angular correlation function: the expectation value of the product of temperatures at pairs of points separated by an angle $\theta$

$$C(\theta) = \left\langle \frac{\Delta T}{T_0}(\vec{n}_1)\frac{\Delta T}{T_0}(\vec{n}_2) \right\rangle = \sum_\ell \frac{(2\ell+1)}{4\pi} C_\ell P_\ell(\cos\theta) \tag{2}$$

where $\cos\theta = \vec{n}_1 \cdot \vec{n}_2$, and $P_\ell$ is the Legendre polynomial of order $\ell$.

The angular power spectrum is defined as the set of $C_\ell$ that verify:

$$< a_{\ell m} a^*_{\ell' m'} >= C_\ell \delta_{\ell\ell'} \delta_{mm'} \tag{3}$$

where $*$ indicates the conjugate.

Experiments measure the $a_{\ell m}$ corresponding to the last scattering surface seen from our position in the Universe. However, the ergodicity property of gaussian fields, allow to determine the angular power spectrum by averaging over the last scattering surface:

$$< |a_{\ell m}|^2 > \approx \frac{\sum_m |a_{\ell m}|^2}{2\ell+1} \tag{4}$$

The power at each $\ell$ is $(2\ell+1)C_\ell/4\pi$. The observing strategy and resolution of each instrument limit the range of angular scales which can be measured as described by the window function [20]:

$$W_\ell(\vec{n}_1, \vec{n}_2) \equiv \int d\vec{m}_1 \int d\vec{m}_2 A(\vec{n}_1, \vec{m}_1) A(\vec{n}_2, \vec{m}_2) P_\ell(\vec{m}_1 \cdot \vec{m}_2) \tag{5}$$

where $\mathrm{A}(\vec{n}_1, \vec{m}_1)$ is the instrument response function to signals coming from direction $\vec{n}_1$ when pointing towards direction $\vec{m}_1$. The particular case $W_\ell(\vec{n}_1, \vec{n}_1)$ is frequently referred as window function. The variance of the observed temperature field, or correlation at zero lag ($\theta = 0$), results

$$< (\frac{\Delta T}{T_0})^2 >= \sum_\ell \frac{(2\ell+1)}{4\pi} C_\ell W_\ell \tag{6}$$

where the window function is denoted as $W_\ell$.

An interferometer provides a direct measurement of the Fourier transform of the intensity distribution on the sky and hence, a determination of the $C_\ell$. For a baseline $d$, the interferometer is sensitive to CMB structure with multipole $\ell = 2\pi d/\lambda$, where $\lambda$ is the wavelength of observations. The instantaneous field of view is determined by the primary beam of the antennas. Comprehensive descriptions of the analysis techniques involved in interferometric observations can be found in the literature (see e.g. [18]). Interferometers with different number of dishes/horns, bandwiths, size of primary beam and approximate multipole range have been used in the search for CMB

anisotropies from various locations [19]. These instruments are rather insensitive to atmospheric distorsion of the microwave signals (see e.g. [21, 22]).

In the early 90s, the Jodrell Bank-IAC 33 GHz interferometer, a pioneer two-element instrument installed at Teide Observatory clearly demonstrated the feasibility of high-sensitivity interferometric measurements of the CMB anisotropy from this site. This precursor of VSA measured CMB fluctuations with amplitude $\Delta T_\ell = 43 \pm 13 \mu K$ and $63 \pm 7 \mu K$ at $\ell = 109$ and 208, respectively [23, 24]. A new generation of CMB interferometers has started operation very recently: the Cosmic Background Imager (CBI, [25]) in the Atacama desert, the Degree Angular Scale Interferometer (DASI, [8]) in Antartic and the Very Small Array (VSA, [26]) in Tenerife have achieved very sensitive measurements of the angular power spectrum in the range $200 \leq \ell \leq 4000$.

# 3 The VSA

The VSA is a purpose-built 14-element radio interferometer (see Figure 1) that has measured the CMB angular power spectrum between $\ell = 150$ and 900 in a compact array configuration [10] and more recently up to $\ell = 1400$ in an extended array configuration [12]. It is located at Teide Observatory (Tenerife) at an altitude of 2340 m. It can operate in the Ka-band ($26 - 36$ GHz), however, to minimize the contribution of foregrounds to the signal recorded it was decided to operate with a bandwidth of 1.5 GHz at the higher end of the band ($\sim$ 33 GHz). Each antenna consists of a conical corrugated horn feeding a paraboloidal mirror and is placed on a 4-m×3-m tip-tilt table surrounded by a metal enclosure to supress as much as possible ground emission. The VSA can observe any sky region between declination $-5^\circ$ and $+60^\circ$. It has been used in two major modes: in the compact configuration, the mirrors were 143-mm in diameter giving a primary beam of $4^\circ.6$ FWHM; in the extended one, the 322-mm diameter apertures allow longer baselines and therefore higher resolutions to be obtained, with a primary beam of $2^\circ$ FWHM. This configuration has a total of 91 baselines with lengths ranging from 0.6 m to 2.5 m, although the maximum possible baseline length, set by the size of the main tip-tilt table, is $\sim$ 4 m. The synthesized beam of a typical VSA field has FWHM $\sim$ 11 arcmin over the primary beam.

Combining all 91 baselines the VSA point source sensitivity is $\sim 6$ Jy $s^{1/2}$. This corresponds to a temperature sensitivity, over a synthesized beam area ($\Omega_{\rm synth} \approx 1 \times 10^{-5}$ sr) of $\sim 15$ mK $s^{1/2}$. The exact value depends on the beam area and on the $u, v$ coverage which in turns depends on the declination and the flagging/filtering of the visibility data.

An important feature of the VSA is the ability to subtract radio sources which contaminate CMB data with a dedicated facility. Combined with map-making capabilities, this makes the VSA ideal for making precise CMB measurements, particularly

Figure 1: The VSA at Teide Observatory.

at higher $\ell$-values.

## 4 Observations

The observations with the compact configuration [27] and the initial three regions observed in the extended configuration [12] are already published. During the period 2001-July 2003 VSA conducted observations of 33 additional pointings with the extended configuration. These pointings conform three 7-field mosaics and four 3-field mosaics giving a total area coverage of 82 sq. degrees. The new observations extend the initial regions with a further 4 pointings per region and incorporate a further 4 new regions each with 3 pointings. This corresponds to a factor of $\sim 4$ in the amount of extended array data and a significant increase in sensitivity over the previous results. Furthermore, the increase in sky-coverage and mosaicing in each field allows an improvement in $\ell$-resolution, or reduced bin-bin correlations, using mosaicing techniques. The total effective integration time is $\approx 6000$ hours (250 days) after filtering and flagging of the data. About $\sim 30$ per cent of data was flagged.

The fields were chosen to avoid as much as possible contamination from Galactic and extragalactic emission. High Galactic latitude ($|b| \geq 27^{\circ}$) fields with low emission as predicted from maps of synchrotron, free-free and dust emission were chosen to minimize Galactic contamination. Fields with bright galaxy clusters were excluded based on existing catalogues [28, 29]. Similarly, fields with bright radio sources ($\geq$ 500 mJy) in the NVSS 1.4 GHz survey [30] and GB6 survey at 4.85 GHz [31] were discarded. Avoiding galaxy clusters is important due to the potential for Sunyaev-Zeldovich Effect (SZE) decrements to contaminate VSA data.

## 5 Data reduction and calibration

The VSA data reduction and calibration procedures are described for the compact and extended configuration in several papers [27, 12]. In [17] full details are given about the reduction of the new extended data. Fourier filtering is used to remove the majority of local undesired signals. The filtering removes typically $10-20$ per cent of the data. The same fringe-rate filtering technique is also applied to the Sun and Moon. Data are filtered if the Sun and Moon are within $27^\circ$ and $18^\circ$ respectively, while if the Sun or Moon are within $9^\circ$ of the field centre then the entire observation is flagged. No residual Sun or Moon contamination was detected after stacking the data typically integrated over $50-100$ days. The data are then further smoothed by a factor of 4 to give 64 sec samples and a correction is applied for the atmospheric contribution to the system noise.

Noise figures vary significantly between baselines, so the final step for each observation is the re-weighting of the data based on the r.m.s. noise of each baseline. This is essential to achieve the optimum overall noise level. The data are then stacked together either in hour angle or in the $u, v$ plane. The final data for each field contains $\sim 10^6$ visibilities, each of 64 sec integration, which are used directly to make maps. For power spectrum estimation, the data are binned in the $u, v$ plane to reduce the number of data points. Each visibility has an associated weight calculated by the reduction pipeline.

The first important step in the calibration of the VSA data is to obtain a precise geometric description of the instrument, i.e. to know the positions for each horne with a precission better than 1/10 the wavelength of observation. This also requires the calculation of corrections for amplitudes, phases and the observing frequency. A maximum-likelihood method [32] is used to solve simultaneously all these parameters. Typically, data from an intense radiosource (like Tau-A) are collected for this purpose. The results are checked via observations of other bright radio sources. Amplitude and phase corrections are usually calculated from a single calibrator for each of the 91 baselines. An unresolved, non-variable bright radio source allows the measured fringes to be corrected for amplitude and phase.

The absolute flux calibration of VSA is made using observations of Jupiter. In the first years of observations we assumed for this planet a brightness temperature $T_{\rm Jup} = 152 \pm 5$ K (3 per cent accuracy in temperature) at 32 GHz [33]. However, data from WMAP gives a more precise determination of the brightness temperature for Jupiter of $T_{\rm Jup} = 146.6 \pm 2.0$ K at 33.0 GHz [34] corresponding to an accuracy of 1.5 per cent in temperature terms, or equivalently 3 per cent in the CMB power spectrum ($\Delta T^2$). We have adopted this WMAP temperature for Jupiter in the calibration of the new extended array data, and consistently scaled our earlier measurements of the power spectrum.

A number of data checks are systematically applied to the data (stacking data in

various ways, splitting in different subsets, non-Gaussian tests to search for residual systematics, etc.), but more importantly, a parallel independent reduction for the majority of the data is performed by the three institutions in the VSA collaboration. The comparison of this independent data reduction showed good agreement for both maps and power spectrum measurements.

# 6 Foregrounds

Radiosources in the fields observed by VSA are first surveyed with the Ryle Telescope at 15 GHz to a limiting flux density of $\sim 10$ mJy [35]. Then these sources are followed with the Source Subtractor (SS), a two-element interferometer located next to the VSA main array operating at the same frequency. It consists of two 3.7 m dishes with a baseline of 9 m providing a resolution of $\sim 3$ arcmin. The observations are conducted simultaneously with VSA, so each source is observed many times during the period of time dedicated to each VSA field. The SS data are calibrated using the flux of the planetary nebula NGC7027, assuming a flux density of $(5.45 \pm 0.20)$ Jy at 32.0 GHz and a flat spectral index $\alpha = 0.1 \pm 0.1$ [33]. The SS flux densities of the sources in the VSA fields are subtracted from the visibility data down to a level of 20 mJy ($\sim 8$ $\mu$K over the synthesized beam area. The complete source survey is presented by [70]. These source counts are also used to re-scale the 30 GHz differential source count model [36] and to make an estimate of the contribution from faint sources below the source subtraction limit of 20 mJy. The residual source power spectrum ($\sim 210$ $\mu$K$^2$ at $\ell = 1000$) is subtracted from the VSA band-power estimates as an uncorrelated statistical correction.

## 6.1 Galactic foregrounds

At the frequency and high angular resolution of the VSA observations it is not expected a significant contribution of the diffuse Galactic foregrounds: synchrotron emission, free-free emission from ionized gas and vibrational dust emission. The power spectrum of these well known foregrounds decreases with increasing $\ell$ [37] and the VSA fields have been selected in regions of high galactic latitude in order to minimize these potential contaminants. Estimates for these foregrounds in the VSA fields have been obtained using three template maps: the 408 MHz all-sky map for synchrotron [38], the H$\alpha$ data from the Wisconsin H-Alpha Mapper (WHAM, [39]) for free-free emission and the 100 $\mu$m map [40] for dust-correlated emission. Similar considerations as in previous work [27] lead to synchrotron and free-free r.m.s. power values for the VSA extended fields of less than (10 $\mu$K$^2$) compared to the CMB fluctuations ($\gtrsim$ 1000 $\mu$K$^2$).

In addition, we have to consider a more controversial foreground, the so called

"foreground X" [41], which appears to be correlated with far infrared dust emission. The characteristics of this foreground have not been fully established yet. Some models [42] predict that spinning dust particles may be the carrier with maximum emission in the range 20-30 GHz. For the dust-correlated component, we smoothed the [40] 100 $\mu$m map to 22 arcmin ($\ell \sim 1000$) and assumed a nominal coupling coefficient between brightness temperature at 33 GHz and the 100 $\mu$m intensity of $T_{\rm b}/I_{100} = 10\ \mu{\rm K}/({\rm MJy\ sr}^{-1})$. This is a nominal value averaged for the high latitude sky. The r.m.s. power fluctuations estimates for the VSA fields range between 1 and 90 $\mu{\rm K}^2$ at $\ell = 1000$, typically $\lesssim 10\ \mu{\rm K}^2$ while the CMB fluctuations are $\Delta T^2_{\rm rms} \sim 1000\ \mu{\rm K}^2$ thus, for most of the VSA regions, the Galactic emission is essentially negligible.

### 6.2 SZ clusters

The VSA fields are selected to avoid known galaxy clusters and minimize any contribution to the CMB temperature from inverse Compton scattering of hot electrons in the intracluster medium, the Sunyaev-Zeldovich (SZ) effect [43, 3]. At the frequency of VSA obsrvations, the SZ effect, produces temperature decrements in the line of sight of the galaxy clusters. The confusion noise produced by a Poisson distribution of unknown high redshift clusters has been estimated using available models [44]. If we adopt $\sigma_8 = 0.9$, we obtain a contribution of $\approx 1$ mJy beam$^{-1}$, approximately six times lower than the noise level in typical VSA maps.

## 7 Results

### 7.1 Maps

The maps are produced using a maximum entropy method (MEM) [45]. The binned visibility data used for deriving the power spectrum are also the starting point for map making. First, the Fourier modes in the $u, v$-plane are reconstructed, then these are Fourier transformed to obtain the maps. The MEM algorithm assumed a flat sky as prior. The signal-to-noise ratio of the maps is in the range SNR$\sim 1-3$, the change being primarily due to the varying integration times after flagging and filtering of the data [17]. The sensitivity of the mosaiced maps is slightly higher than this, due to the overlapping of the individual fields.

The VSA maps allow a comparison to be made with other CMB data. The recent WMAP data release [14] has provided 5 all-sky maps at frequencies centred at 22.8 (K-band), 33 (Ka-band), 40.7 (Q-band), 60.8 (V-band) and 93.5 GHz (W-band) with resolutions ranging from 49.2 arcmin (K-band) to 12.6 arcmin (W-band). The signal-to-noise ratio of WMAP data at the VSA resolution is $\sim 1$ and hence much of the CMB signal is lost in the noise. The actual noise level in the WMAP data depends on

position due to the scanning strategy of the WMAP satellite. For the 1-year WMAP data release, the noise is $\sim 100 - 200$ $\mu$K per 12.6 arcmin pixel in the VSA regions, compared to $\sim 20$ $\mu$K beam$^{-1}$ in the VSA mosaiced maps.

## 7.2 Power spectrum

The final visibility data are binned into $u, v$ square cells, each 9 wavelengths on a side, to oversample the data. This reduces the number of data points by a factor of $\gtrsim 1000$. Sources are subtracted using position and flux density information from the Source Subtractor. For each VSA pointing there is a final visibility file with $\sim 10^3$ data points.

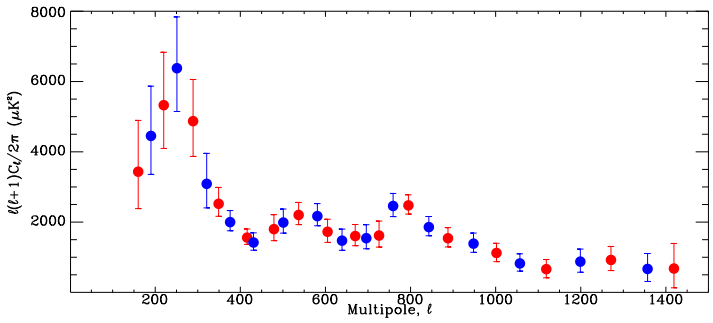


Figure 2: The CMB power spectrum as measured by the VSA by combining the data from all 7 VSA regions [17]. The first 3 bins are included from earlier VSA data in a compact array. The errors represent 1 $\sigma$ limits. Two alternate binnings (grey and black) are displayed. Absolute calibration is accurate to 3 per cent and is not included in the errors.

The binned visibilities form the basic input to the maximum likelihood analysis for the CMB power spectrum. We used the Microwave Anisotropy Dataset Computational sOftWare (MADCOW) [46] which can deal with mosaiced observations and variable bin-widths.The band powers calculated from the complete VSA data set, both the compact and extended arrays are available at the following URL:
`http://www.jb.man.ac.uk/research/vsa/vsa_results.html.`
The extended array data have little sensitivity at $\ell \lesssim 300$. The 3 bins at $\ell < 300$ are therefore dominated by data from the compact array [10]. The error bars were calculated from the probability likelihood functions by enclosing 68 per cent of the area centred on $\ell_h$, the median $\ell$ value for each bin. Calibration uncertainty ($\approx 3$ per cent) is not included. Sample variance is included in the error estimates. The

VSA power spectrum (Figure 2) clearly shows the existence of the first three acoustic peaks and the fall-off in power towards higher $\ell$.

# 8 Cosmological implications

We first consider the standard six-parameter flat ΛCDM model, and then include extra parameters as in the approach adopted by the WMAP team [16, 47, 48]. In the case where we do not impose external priors on the CMB data (WMAP+VSA), we find that there is significant evidence ($> 2\sigma$) for negative running; something which is not implied by the WMAP data alone. The significance of this result is sensitive to the inclusion of external priors, the relative calibration of WMAP and VSA, and possible source/cluster contamination of the measured power spectrum. Second, we consider a 12-parameter model fit to WMAP, WMAP+VSA and all available CMB data beyond $\ell > 1000$, illustrating the effects of external priors on the estimated parameters.

## 8.1 Methodology

### Cosmological model

The ΛCDM model assumes that the Universe is flat and dominated by cold dark matter (CDM), baryons and a cosmological constant, Λ. The densities of these components relative to critical are denoted $\Omega_{\rm dm}$, $\Omega_{\rm b}$ and $\Omega_\Lambda$ respectively and we define $\Omega_{\rm m} = \Omega_{\rm dm} + \Omega_{\rm b}$ to be the overall matter density (CDM and baryons) in the same units. The expansion rate is quantified in terms of the Hubble constant $H_0 = 100h\,{\rm km\,sec^{-1}\,Mpc^{-1}}$ and we allow for instantaneous reionization at some epoch $z_{\rm re}(< 30)$ which can also be quantified in terms of an optical depth $\tau$. The so-called physical densities of the CDM and baryons are defined as $\omega_{\rm dm} = \Omega_{\rm dm}h^2$ and $\omega_{\rm b} = \Omega_{\rm b}h^2$. We will consider only adiabatic models and parameterize the initial fluctuation spectrum of this model by

$$P(k) = A_{\rm S}\left(\frac{k}{k_{\rm c}}\right)^{n_{\rm S}}, \qquad (7)$$

where $k_{\rm c} = 0.05{\rm Mpc}^{-1}$ is the arbitrarily chosen pivot point of the spectrum, $n_{\rm S}$ is the spectral index and $A_{\rm S}$ is the scalar power spectrum normalization.

We will also consider a model with a running spectral index,

$$P(k) = A_{\rm S}\left(\frac{k}{k_{\rm c}}\right)^{n_{\rm S}+\frac{1}{2}n_{\rm run}\log(k/k_{\rm c})}, \qquad (8)$$

so that the overall spectral index of fluctuations is a function of scale, $n_{\rm S}(k)$, given by

$$n_{\rm S}(k) = \frac{d(\log\, P)}{d(\log\, k)} == n_{\rm S} + n_{\rm run} \log\left(\frac{k}{k_{\rm c}}\right) , \qquad (9)$$

where $n_{\rm run}$ is known as the running of the spectral index. For slow roll inflation to be well defined, one requires that $|n_{\rm run}| \ll |1-n_{\rm S}|/2$ [49]. Under certain choices of priors we find that there is some evidence that this inequality is violated by the preferred fits to the data.

The other parameters which we will consider in our analyses are: $f_\nu = \Omega_\nu/\Omega_{\rm dm}$, the fraction of the dark matter which is massive neutrinos; $\Omega_{\rm k} = 1 - \Omega_{\rm tot}$ ($\Omega_{\rm tot} = \Omega_{\rm dm} + \Omega_{\rm b} + \Omega_\nu + \Omega_\Lambda$), the curvature in units of the critical density; $w = P_{\rm Q}/\rho_{\rm Q}$, the equation-of-state parameter for a dark energy component modelled as a slowly rolling scalar field; $n_{\rm T}$ the spectral index of tensor fluctuations specified at the pivot point $k_{\rm c} = 0.002\,{\rm Mpc}^{-1}$; $R = A_{\rm T}/A_{\rm S}$, the ratio of the amplitude of the scalar fluctuations, $A_{\rm S}$, evaluated at $k_{\rm c} = 0.05\,{\rm Mpc}^{-1}$, and that of the tensor fluctuations evaluated at $k_{\rm c} = 0.002\,{\rm Mpc}^{-1}$. In addition to these parameters, for which we fit, we will also comment on various derived quantities: $t_0$, the age of the universe; $\sigma_8$, the amplitude of density fluctuations in the spheres of $8h^{-1}\,{\rm Mpc}$.

## 8.2 CMB data

Four different combinations of CMB data have been considered.

- The first data set, denoted COBE+VSA contains the VSA data as described in the previous sections [17] combined with the COBE data [4, 50].
- The second data set, denoted WMAP contains only the WMAP temperature (TT) data [15] and temperature-polarization cross-correlation (TE) data [51].
- The third data set contains WMAP data and the new VSA data and is referred to as WMAP+VSA. This allows to illustrate the relevance of measurements of the power spectrum on small angular scales.
- Finally, we combine the previous two with all important CMB experiments providing measurements in the region of the second peak of the spectrum and beyond, namely CBI, ACBAR, Boomerang, Maxima, DASI [11, 13, 7, 52, 8]. This last data set is hereafter referred to as AllCMB.

### External priors

In addition to the CMB data sets described above, we consider the effects of other cosmological data, not only to break the degeneracies, but also to see how the mea-

sured CMB power spectrum fits in the wider cosmological context. The external priors used are:

- The constraint on the expansion rate of the Universe from the Hubble Space Telescope (HST) Key project value of $H_0 = 72 \pm 8\,\mathrm{km\,sec^{-1}\,Mpc^{-1}}$ [53]. The error-bar includes both statistical and systematic uncertainty.
- Constraints on large scale structure from the 2dF Galaxy Redshift Survey [54, 55, 56], which provides measurements on scales $0.02 < k/(h\,\mathrm{Mpc^{-1}}) < 0.15$.
- Constraints from Type Ia Supernovae (SNeIa) [57, 58].
- Constraints from the gas fraction ($f_{gas}$) in dynamically relaxed clusters of galaxies [59] and from the observed local X-ray luminosity function (XLF) of galaxy clusters [60].
- Constraints from cosmic shear (CS) measurements [61].

**Parameter estimation**

The parameter estimation has been performed using the COSMOMC software package [62]. The calculations were performed on LAM clusters with a total of 42 CPUs at the IAC in La Laguna, Tenerife and the COSMOS supercomputer facility at the University of Cambridge. The COSMOMC software uses the Markov Chain Monte Carlo (MCMC) algorithm to explore the hypercube of parameters on which we impose flat priors. These priors are listed in Table 8.2. Additionally, the software automatically imposes the physical prior $\Omega_\Lambda > 0$, which can significantly affect the marginalized probability distributions (see [63] for further discussion).

## 8.3 Flat ΛCDM models

**Standard six-parameter model**

We begin our discussion in the context of the standard flat ΛCDM model with six free parameters ($\omega_\mathrm{b}$, $\omega_\mathrm{dm}$, $h$, $n_\mathrm{S}$, $A_\mathrm{S}$, $\tau$) with no external priors.

The constraints derived for the parameters are tabulated in Table 8.3. The values for WMAP alone can be compared with those in [16]. Noting that they present $\omega_\mathrm{m} = \Omega_\mathrm{m} h^2$, instead of $\omega_\mathrm{dm}$, there are only minor discrepancies in the central values, although some of the limits appear to be somewhat larger. The preferred value of the redshift of reionization is $z_\mathrm{re} = 17^{+8}_{-6}$. The inclusion of the high-resolution data from the VSA modifies the limits on each of the parameters and these are most significant for $n_\mathrm{S}$, whose best fitting value reduces from 1.00 to 0.97. The result for $n_\mathrm{S}$ will be central to our subsequent discussion of the primordial power

| Basic Parameter | Prior |
|---|---|
| $\omega_{\rm b}$ | (0.005,0.10) |
| $\omega_{\rm dm}$ | (0.01, 0.99) |
| $h$ | (0.4,1.0) |
| $n_{\rm S}, n_1, n_2$ | (0.5,1.5) |
| $z_{\rm re}$ | (4,30) |
| $10^{10}A_{\rm S}$ | (10,100) |
| $n_{\rm run}$ | $(-0.15,0.15)$ |
| $A_{\rm X}/(\mu{\rm K})^2$ | $(-500,500)$ |
| $f_\nu$ | (0,0.2) |
| $\Omega_{\rm k}$ | $(-0.25,0.25)$ |
| $w$ | $(-1.5,0)$ |
| $R$ | (0,2) |
| $n_{\rm T}$ | $(-1.5,3)$ |

Table 1: Priors used on each cosmological parameter when it is allowed to vary. The notation $(a, b)$ for parameter $x$ denotes a top-hat prior in the range $a \leq x \leq b$.

| Parameter | COBE+VSA | WMAP | WMAP+VSA |
|---|---|---|---|
| $\omega_{\rm b}$ | $0.0328^{+0.0073}_{-0.0071}$ | $0.0240^{+0.0027}_{-0.0016}$ | $0.0234^{+0.0019}_{-0.0014}$ |
| $\omega_{\rm dm}$ | $0.125^{+0.031}_{-0.027}$ | $0.117^{+0.018}_{-0.018}$ | $0.111^{+0.014}_{-0.016}$ |
| $h$ | $0.77^{+0.15}_{-0.17}$ | $0.73^{+0.10}_{-0.06}$ | $0.73^{+0.09}_{-0.05}$ |
| $n_{\rm S}$ | $1.05^{+0.12}_{-0.08}$ | $1.00^{+0.09}_{-0.04}$ | $0.97^{+0.06}_{-0.03}$ |
| $10^{10}A_{\rm S}$ | $25^{+11}_{-6}$ | $27^{+9}_{-5}$ | $23^{+7}_{-3}$ |
| $\tau$ | Unconstrained | $0.18^{+0.16}_{-0.08}$ | $0.14^{+0.14}_{-0.07}$ |

Table 2: Parameter estimates and 68% confidence limits for the standard six-parameter flat ΛCDM model.

| CMB | External | $n_{\rm S}$ | $n_{\rm run}$ |
|---|---|---|---|
| COBE+VSA | None | $0.93^{+0.13}_{-0.12}$ | $-0.081^{+0.049}_{-0.049}$ |
| WMAP | None | $0.94^{+0.07}_{-0.06}$ | $-0.060^{+0.037}_{-0.036}$ |
| WMAP+VSA | None | $0.96^{+0.07}_{-0.07}$ | $-0.069^{+0.032}_{-0.032}$ |
| COBE+VSA | HST | $0.92^{+0.11}_{-0.12}$ | $-0.081^{+0.048}_{-0.048}$ |
| WMAP | HST | $0.95^{+0.06}_{-0.07}$ | $-0.060^{+0.037}_{-0.037}$ |
| WMAP+VSA | HST | $0.93^{+0.06}_{-0.05}$ | $-0.069^{+0.036}_{-0.036}$ |
| COBE+VSA | 2dF | $1.00^{+0.12}_{-0.13}$ | $-0.044^{+0.058}_{-0.061}$ |
| WMAP | 2dF | $0.95^{+0.05}_{-0.06}$ | $-0.038^{+0.025}_{-0.037}$ |
| WMAP+VSA | 2dF | $0.93^{+0.05}_{-0.05}$ | $-0.049^{+0.035}_{-0.034}$ |

Table 3: Limits on $n_{\rm S}$ and $n_{\rm run}$ in the flat ΛCDM model with a running spectral index for different CMB data sets and external priors.

spectrum. The results from WMAP+VSA are very similar to those presented in [16] for WMAP+ACBAR+CBI. We also find a larger value for $\omega_{\rm b}$ than suggested by WMAP, WMAP+VSA and standard Big Bang Nucleosynthesis, $\omega_{\rm b} = 0.020 \pm 0.002$, [64].

**Running spectral index models**

In the previous section we saw that the inclusion of the VSA data to that of WMAP shifts the derived limits on the spectral index. Standard, slow-roll models of inflation predict that the spectral index will be a function of scale, albeit at a very low level, and it seems a sensible parameter to allow as the first beyond the standard model. The analysis of [16, 48] provided evidence for a non-zero value of $n_{\rm run} (= -0.031^{+0.016}_{-0.017})$ when using CMB data from WMAP, ACBAR and CBI, along with large-scale structure data

from the 2dF galaxy redshift survey and the Lyman-$\alpha$ forest.

We will start our discussion by considering the same model as in the previous section with no external priors, but with $n_{\rm run}$ allowed to vary. The derived limits on $n_{\rm S}$ and $n_{\rm run}$ are presented in the first three rows of Table 8.3 for COBE+VSA, WMAP and WMAP+VSA. The derived limits on $\omega_{\rm b}$, $\omega_{\rm dm}$ and $h$ are not changed appreciably and the other parameters, $A_{\rm S}$ and $\tau$ (or $z_{\rm re}$) are strongly degenerate and $z_{\rm re}$ will feature in our discussion below.

The values of $n_{\rm S}$ and $n_{\rm run}$ are not particularly well constrained by COBE+VSA, but it is worth noting that even in this case there is a definite preference for a value of $n_{\rm run} < 0$. The results have been included for completeness and provide a useful cross-check. The results for WMAP are somewhat different to those presented in [16]. In particular we find that $n_{\rm run} = -0.060^{+0.037}_{-0.036}$, a $1.6\sigma$ preference for $n_{\rm run} < 0$, as opposed to $n_{\rm run} = -0.047 \pm 0.04$ from Spergel et al. [16]. The significance of this result is improved to $2.2\sigma$ by the inclusion of the high resolution data from the VSA. We remark that this result comes from CMB data alone.

We have tested the sensitivity of this apparently result to the inclusion of external priors from the HST and 2dF galaxy redshift survey, and the results are also presented in Table 8.3. We see that the effect of the HST prior is to relax marginally the constraint on $n_{\rm run}$, although there is a significant change in the derived limit on $n_{\rm S}$. We note that the results for WMAP alone are very similar with and without the HST prior. The inclusion of 2dF does significantly affect our results. Using just WMAP we find that there is only a marginal preference for $n_{\rm run} < 0$ and the inclusion of VSA only yields a $1.4\sigma$ result. We note that this is a shift in the derived value and the error bars do not change significantly.

We have also considered the effects of including other CMB information from the two other high resolution experiments ACBAR and CBI. We find that the inclusion of their results does not appear to be as significant as the VSA in preferring a value of $n_{\rm run} < 0$ and that the result of considering WMAP+ACBAR+CBI+VSA is very similar to just WMAP+VSA. We note that the ACBAR and CBI experiments quote large global calibration uncertainties (20% and 10% in power), which we believe is at least as responsible for this result as their errors on the individual power spectrum band powers.

**Neutrino fraction**

As a final extension to our flat ΛCDM model, it is of interest to include the fraction $f_\nu$ of dark matter in the form of neutrinos. Evidence for a neutrino oscillation, and hence for the existence of massive neutrinos, has been found by solar neutrino and atmospheric neutrino experiments [65, 66, 67, 68]. Further evidence for a non-zero value of the neutrino mass has recently been claimed from cosmological data [69].

In addition to obtaining constraints on $f_\nu$, the inclusion of this parameter will

inevitably lead to some broadening of the marginalized distributions for the other parameters. Of particular interest is whether the constraints on the running spectral index derived above are robust to the inclusion of $f_\nu$. We therefore include $f_\nu$, with the top-hat prior given in Table 8.2, into the running spectral index model. In the analysis of this model, we include the 2dF external prior, since current CMB alone provide only a weak constraint on $f_\nu$.

We find that the 95% upper limit provided by the COBE+VSA data set, $f_\nu < 0.132$, is only marginally larger than that obtained using WMAP data, $f_\nu < 0.090$. The combination WMAP+VSA gives similar limits to WMAP, namely $f_\nu < 0.087$, which corresponds to neutrino mass of $m_\nu < 0.32$eV when the neutrino masses are degenerate.

For the parameters $n_{\rm S}$ and $n_{\rm run}$, the marginalized distributions have indeed been shifted and broadened by the inclusion of $f_\nu$ although the effects are not very strong. In particular, we note that our earlier finding of a preference for a non-zero value of $n_{\rm run}$ has been weakened somewhat. A non-zero $n_{\rm run}$ is still preferred, but at reduced significance. For the WMAP+VSA data set, we obtain $n_{\rm S} = 0.94^{+0.06}_{-0.06}$ and $n_{\rm run} = -0.041^{+0.037}_{-0.036}$ with 68% confidence limits.

In the above analysis we used only 2dF as an external prior. It is of interest to investigate the effect of including different combinations of the additional external priors listed in Table 8.2. The effect of these additional priors has been calculated by importance sampling our previous results. We also investigate the effect of including all recent CMB data into our analysis. In Figure 3, we plot confidence limits on all the model parameters for each of our four CMB data sets, each of which, in turn, includes four different combinations of external priors: 2dF, 2dF+$f_{\rm gas}$, 2dF+$f_{\rm gas}$+XLF, 2df+HST and 2dF+CS. The points indicate the median of the corresponding marginalized distribution, and the error bars show the 68% central confidence limit. If the distribution peaks at zero, the point is placed on the axis and the 95% upper limit is shown.

We see that the inclusion of the $f_{\rm gas}$ and XLF external priors significantly reduces the error bars on all parameters. The most profound effect is obtained from the XLF prior for the parameters $f_\nu$, $\sigma_8$ and $z_{\rm re}$, as might be expected from [69]. Indeed, it is only with the inclusion of the XLF prior that a non-zero value of $f_\nu$ is preferred and only then at limited significance. For each of the CMB data set combinations, the best-fitting value in this case is $f_\nu \approx 0.05$, which corresponds to neutrino mass of $m_\nu \approx 0.18$eV when the neutrino masses are degenerate, with a zero value excluded at around 96% confidence. For $\sigma_8$ the inclusion of the XLF prior significantly reduces the best-fit value and the error bars for all CMB data set combinations. A similar, but less pronounced, effect is seen for $z_{\rm re}$.

| | WMAP | WMAP+VSA | AllCMB |
|---|---|---|---|
| $\Omega_{\rm b}h^2$ | $0.025^{+0.003}_{-0.003}$ | $0.024^{+0.003}_{-0.002}$ | $0.023^{+0.002}_{-0.002}$ |
| $\Omega_{\rm dm}h^2$ | $0.108^{+0.022}_{-0.021}$ | $0.111^{+0.021}_{-0.019}$ | $0.113^{+0.017}_{-0.017}$ |
| $h$ | $0.66^{+0.07}_{-0.06}$ | $0.66^{+0.06}_{-0.06}$ | $0.65^{+0.07}_{-0.07}$ |
| $z_{\rm re}$ | $18^{+7}_{-7}$ | $19^{+7}_{-7}$ | $17^{+7}_{-8}$ |
| $\Omega_{\rm k}$ | $-0.02^{+0.03}_{-0.03}$ | $-0.01^{+0.03}_{-0.03}$ | $-0.02^{+0.03}_{-0.03}$ |
| $f_\nu$ | $< 0.093$ | $< 0.083$ | $< 0.083$ |
| $w$ | $-1.00^{+0.24}_{-0.27}$ | $-0.99^{+0.24}_{-0.27}$ | $-1.06^{+0.24}_{-0.25}$ |
| $n_{\rm S}$ | $1.04^{+0.12}_{-0.11}$ | $0.99^{+0.09}_{-0.09}$ | $0.96^{+0.07}_{-0.07}$ |
| $n_{\rm T}$ | $0.26^{+0.53}_{-0.60}$ | $0.13^{+0.49}_{-0.51}$ | $0.12^{+0.48}_{-0.51}$ |
| $n_{\rm run}$ | $-0.02^{+0.07}_{-0.05}$ | $-0.04^{+0.05}_{-0.04}$ | $-0.04^{+0.04}_{-0.05}$ |
| $10^{10}A_{\rm S}$ | $27^{+8}_{-5}$ | $26^{+9}_{-5}$ | $25^{+6}_{-5}$ |
| $R$ | $< 0.78$ | $< 0.77$ | $< 0.68$ |
| $\Omega_\Lambda$ | $0.71^{+0.07}_{-0.09}$ | $0.70^{+0.06}_{-0.08}$ | $0.69^{+0.07}_{-0.09}$ |
| $t_0$ | $14.1^{+1.4}_{-1.1}$ | $14.1^{+1.3}_{-1.2}$ | $14.4^{+1.4}_{-1.3}$ |
| $\Omega_{\rm m}$ | $0.31^{+0.09}_{-0.07}$ | $0.31^{+0.08}_{-0.06}$ | $0.33^{+0.10}_{-0.07}$ |
| $\sigma_8$ | $0.76^{+0.14}_{-0.14}$ | $0.77^{+0.13}_{-0.13}$ | $0.76^{+0.11}_{-0.12}$ |
| $\tau$ | $0.20^{+0.13}_{-0.11}$ | $0.20^{+0.15}_{-0.10}$ | $0.17^{+0.12}_{-0.10}$ |

Table 4: Parameter estimates and 68% confidence intervals for various cosmological parameters. For $f_\nu$ and $R$, the 95% upper limits are quoted.

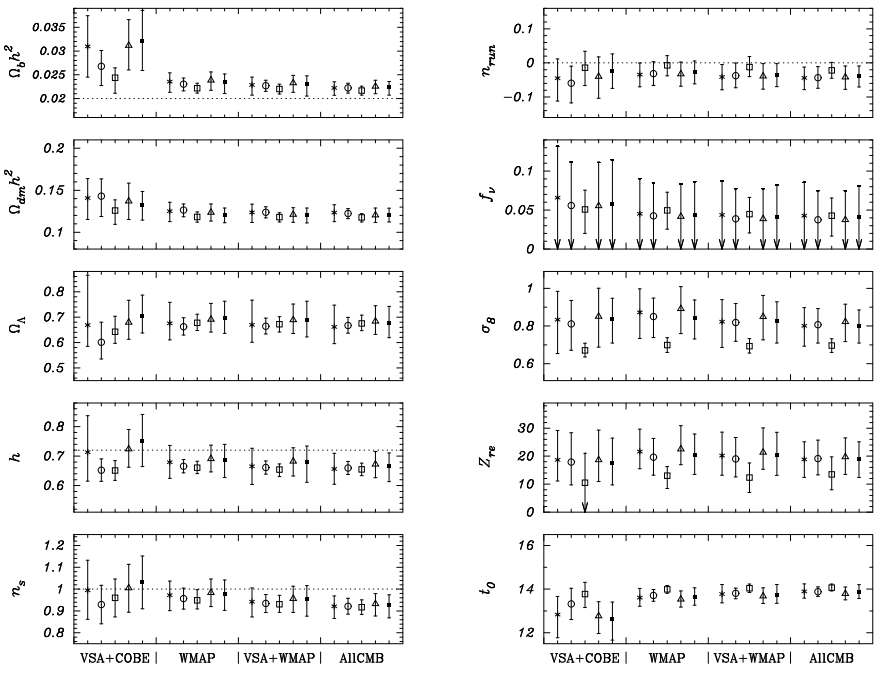


Figure 3: Estimates for cosmological parameters in the flat ΛCDM running spectral index model, extended to include $f_\nu$. Four CMB data sets are considered and, for each data set, four determinations are plotted, corresponding to different combinations of external priors. From left to right the external priors are: 2dF; 2dF+$f_{\rm gas}$; 2dF+$f_{\rm gas}$+XLF; 2dF+HST and 2dF+CS. The points indicate the median of the corresponding marginal distributions. The error bars denote 68% confidence limits. If a distribution peaks at zero then the 95% upper limit is shown. The horizontal dashed lines plotted in some of the panels indicate BBN values for $\Omega_{\rm b}h^2$, the value of $h$ given by the HST key project, the Harrison-Zeldovich value of the spectral index of fluctuations and a zero value for the running index.

### 8.4 General ΛCDM model

Thus far we have considered only a limited range of flat ΛCDM models. In principle, one should properly include all the relevant unknowns into the analysis in order to obtain conservative confidence limits. In this section, we consider a more general ΛCDM model. In addition to including $f_\nu$ and $n_{\rm run}$, the standard six-parameter flat ΛCDM model is further extended by including $\Omega_k$, $w$, $R = A_{\rm T}/A_{\rm S}$ and $n_{\rm T}$. This gives 12 variable parameters in total, for which we adopt the top-hat priors listed in Table 8.2.

For this model, we consider the three CMB data sets WMAP, WMAP+VSA and AllCMB. In addition, we now use both 2dF and SNeIa as our basic external priors, which are required in order to set constraints on our 12-dimensional cosmological parameter space. The corresponding confidence limits on the parameter values are given in Table 8.3.

For $\Omega_{\rm b}h^2$ we see a clear trend towards a lower preferred value (closer to the BBN estimate) as one adds first VSA data and then all remaining CMB data sets. This effect is accompanied by a gradual upwards trend in the preferred $\Omega_{\rm dm}h^2$ value. The other parameters exhibiting such trends are $n_{\rm S}$ and $n_{\rm run}$. As more CMB data are included, the preferred value of $n_{\rm S}$ moves slightly below unity, although this value is by no means excluded. Perhaps more importantly, the upper limit on $n_{\rm S}$ is significantly reduced as more CMB data are added. An analogous effect is observed for $n_{\rm run}$, for which the addition of VSA data significantly reduces the tail of the distribution for positive values of $n_{\rm run}$.

We see that the inclusion of the $f_{\rm gas}$ and XLF external priors has the greatest effect on the confidence limits, and that this is most pronounced for the XLF prior and the parameters $f_\nu$, $\sigma_8$ and $z_{\rm re}$. It is reassuring, however, that the derived limits on $f_\nu$ for the general model are very similar to those obtained assuming the simpler flat model. We again find $f_\nu \approx 0.05$, with a zero-value excluded at about 92% confidence which is slightly lower than for the flat case. The effect of the XLF prior on $\sigma_8$ and $z_{\rm re}$ in the general model is also similar to that observed in the simpler flat case.

## 9 Conclusions

We have used recent data from the Very Small Array, together with other CMB datasets and external priors, to set constraints on cosmological parameters. We have considered both flat and non-flat ΛCDM models and the results are consistent.

Within the flat ΛCDM model, we find that the inclusion of VSA data suggests that the initial fluctuation spectrum that is not described by a single power-law. The negative running, which reduces the amount of power on small scales and hence the amount of structure at early times, leads to predictions for the epoch of reionization at odds with the best fit to the CMB data. We shall caution that this result may

be affected by the absolute calibration uncertainty of the VSA power spectrum and the residual point source correction due to sources below out subtraction limit of 20mJy. It is possible that an imperfect subtraction, either an over-estimate or an under-estimate, could lead to inaccuracies in the derived limits on the cosmological parameters, in particular on $n_{\rm S}$ and $n_{\rm run}$.

For the general 12-parameter ΛCDM model, we find that our marginalized distributions for $n_{\rm S}$ and $n_{\rm run}$ are broadened, as one would expect. Nevertheless, even in this case, the addition of VSA data significantly reduces tails of the distributions for $n_{\rm S}$ greater than unity and for positive $n_{\rm run}$, as compared with using WMAP as the only CMB data set. Indeed, these effects are reinforced by the use of the AllCMB data set. The inclusion of additional CMB data beyond WMAP also leads to a noticeable reduction in the preferred value of $\omega_{\rm b}$ and a corresponding increase in $\omega_{\rm dm}$.

To summarize, we find that there is evidence for $n_{\rm run} < 0$ in a limited class of models, but within the general ΛCDM model with 12 parameters the evidence is much weaker. Standard models of inflation are generally incompatible with such large negative values of $n_{\rm run}$, but the data appears to point in that direction, although not totally conclusively. The inclusion of an external prior from 2dF appears to weaken the result by fixing $\Omega_{\rm m} \approx 0.3$ in conjunction with the CMB data. The measurement of $\Omega_{\rm m}h$ using the galaxy power spectrum is responsible for this shift. It is an interesting question as to how reliable this measurement is since a slight shift in the results, a preference for $\Omega_{\rm m}h \approx 0.17$ rather than $\Omega_{\rm m}h \approx 0.21$ would bring their preferred value into line with that suggested by the CMB alone and would uphold the possibility of $n_{\rm run} < 0$. Since none of the galaxy redshift surveys have conclusively observed the turnover in the power spectrum on which this determination of $\Omega_{\rm m}h$ is based we assert that there is still room for some doubt. We set an upper limit on the mass of each of the three neutrino flavours of $m_\nu < 0.32$eV (95 C.L.). We have shown that measurements of the CMB power spectrum beyond $\ell = 1000$ can have an impact on the estimation of cosmological parameters and that future measurements in this region by the VSA, the PLANCK satellite and others will enable us in the future to make more definitive statements.

*Acknowledgements:* We thank the staff of Jodrell Bank Observatory, Mullard Radio Astronomy Observatory and IAC for assistance in the day-to-day operation of the VSA. We thank PPARC and the IAC for funding and supporting the VSA project. Partial financial support was provided by Spanish Ministry of Science and Technology project AYA2001-1657.

## References

[1] Fixen, D. J., Cheng, E. S., Gales, J. M., Mather, J. C., Shafer, R. A., Wright, E. L. 1996, ApJ, 473, 576

[2] Peebles, P.J.E. and Yu, J. T. 1970, ApJ, 162, 815
[3] Sunyeav, R. A., Zeldovich, Y. B. 1970, ApJSS, 7, 3
[4] Smoot G. F. et al. 1992, ApJ, 396, L1
[5] de Bernardis, P. et al. 2000, Nature, 404, 955
[6] Lee A. T. et al. 2001, ApJ, 561, L1
[7] Netterfield C. B. et al. 2002, ApJ, 571, 604
[8] Halverson N. W. et al. 2002, ApJ, 568, 38
[9] Benoît A. et al. 2003, A&A, 399, L19
[10] Scott P. F. et al. 2003, MNRAS, 341, 1076
[11] Pearson T. J. et al. 2003, ApJ, 591, 556
[12] Grainge K.J.B. et al. 2003, MNRAS, 341, L23
[13] Kuo C. L. et al. 2004, ApJ, 600, 32
[14] Bennett C. L. et al. 2003a, ApJSS, 148, 1
[15] Hinshaw, G. et al. 2003a, ApJSS, 148, 135
[16] Spergel D. N. et al. 2003, ApJSS, 148, 175
[17] Dickinson C. et al. 2004, MNRAS, submitted
[18] White, M., Carlstrom, J. E., Dragovan, M., and Holzapfel, W. L. 1999, ApJ, 514, 12
[19] Rebolo R. 2002, Space Sci. Rev., 100, 15
[20] White, M., Srednicki, M. 1995, ApJ, 443, 6
[21] Webster, A. 1994, MNRAS, 268, 299
[22] Church, S. E. 1995, MNRAS, 272, 551
[23] Dicker, S. R., Melhuish, S. J., Davies, R. D., Gutiérrez, C. M., Rebolo, R., Harrison, D. L., Davis, R. J., Wilkinson, A., Hoyland, R. J., Watson, R.A. 1999, MNRAS, 309, 750
[24] Harrison, D. L., Rubiño-Martín, J. A., Melhuish, S. J., Watson, R.A., Davies, R.D., Rebolo, R., Davis, R. J., Gutiérrez, C. M., Macías-Pérez 2000, MNRAS, 316, L24
[25] Padin et al. 2001, ApJ, 549, L1
[26] Watson R. A. et al. 2003, MNRAS, 341, 1057
[27] Taylor A. C. et al. 2003, MNRAS, 341, 1066
[28] Ebeling, H., Edge, A. C., Böhringer, H., Allen, S. W., Crawford, C. S., Fabian, A. C., Voges, W., Huchra, J. P. 1998, MNRAS, 301, 881
[29] Abell G. O. 1958, ApJSS, 3, 211
[30] Condon, J. J., Cotton, W. D., Greisen, E. W., Yin, Q. F., Perley, R. A., Taylor, G. B., Broderick, J. J. 1998, AJ, 115, 1693
[31] Gregory, P. C., Scott, W. K., Douglas, K., Condon, J. J. 1996, ApJSS, 103, 427
[32] Maisinger, K., Hobson, M. P., Saunders, R.D.E., Grainge, K.J.B. 2003, MNRAS, 345, 800
[33] Mason, B. S., Leitch, E. M., Myers, S. T., Cartwright, J. K., Readhead, A.C.S. 1999, AJ, 118, 2908
[34] Page L. et al. 2003, ApJSS, 148, 39

[35] Waldram, E. M., Pooley, G. G., Grainge, K.J.B., Jones, M. E., Saunders, R.D.E., Scott, P. F., Taylor, A. C. 2003, MNRAS, 342, 915
[36] Toffolatti, L., Argueso Gomez, F., de Zotti, G., Mazzei, P., Franceschini, A., Danese, L., Burigana, C. 1998, MNRAS, 297, 117
[37] Giardino, G., Banday, A.J., Fosalba, P., Górski, K. M., Jonas, J. L., O'Mullane, W., Tauber, J. 2001, A&A, 371, 708
[38] Haslam, C.G.T., Klein, U., Salter, C. J., Stoffel, H., Wilson, W. E., Cleary, M. N., Cooke, D. J., Thomasson, P. 1981, A&A, 100, 209
[39] Haffner, L. M., Reynolds, R. J., Tufte, S. L., Madsen, G. J., Jaehnig, K. P., Percival, J. W. 2003, ApJSS, 149, 405
[40] Schlegel, D. J., Finkbeiner, D. P., Davis, M. 1998, ApJ, 500, 525
[41] de Oliveira-Costa, A., Tegmark, M., Davies, R. D., Gutiérrez, C. M., Lasenby, A. N., Rebolo, R., Watson, R. A., ApJ, submitted (astro-ph/0312039)
[42] Draine, B. T., Lazarian, A. 1998, ApJ, 494, L19
[43] Zeldovich, Y. B., Sunyaev, R. A. 1969,ApJSS, 4, 301
[44] Battye, R. A., Weller, J. 2003, Phys. Rev. D, 68, 083506
[45] Maisinger, K., Hobson, M. P., Lasenby, A. N. 1997, MNRAS, 290, 313
[46] Hobson, M. P., Maisinger, K. 2002, MNRAS, 334, 569
[47] Verde L. et al. 2003, ApJSS, 148, 195
[48] Peiris, H. V. et al. 2003, ApJSS, 148, 213
[49] Leach, S., Liddle, A. R. 2003, astro-ph/0306305
[50] Bennett, C. L. et al. 1996, ApJ, ApJ, 464, L1
[51] Kogut A. et al. 2003, ApJSS, 148, 161
[52] Hanany S. et al. 2002, ApJ, 545, L5
[53] Freedman W. L. et al. 2001, ApJ, 553, 47
[54] Colless M. et al 2001, MNRAS, 328, 1039
[55] Percival W. J. et al. 2001, MNRAS, 327, 1297
[56] Percival W. J. et al. 2002, MNRAS, 337, 1068
[57] Perlmutter S. et al. 1999, ApJ, 517, 565
[58] Reiss A. et al. 1998, AJ, 116, 1009
[59] Allen, S., Schmidt, R. W., Fabian, A. C. 2002, MNRAS, 334, L11
[60] Allen, S., Schmidt, R. W., Fabian, A. C., Ebeling, H. 2003a, MNRAS, 342, 287
[61] Hoekstra, H., Yee, H.K.C., Gladders, M. D. 2002, ApJ, 577, 595
[62] Lewis, A. L., Bridle S. L. 2002, PRD, 66, 103511
[63] Slosar, A. et al. 2003, MNRAS, 341, L29
[64] Burles, S., Nollett, K. M., Turner, M. S. 2001,ApJ, 552, L1
[65] Fukuda Y. et al. 1998, Phys. Rev. Lett., 81, 1562
[66] Fukuda Y. et al. 2002, Phys. Lett. B, 539, 179
[67] Allison W.W.M. et al. 1999, Phys. Lett. B, 449, 137
[68] Ambrosio M. et al 2000, Phys. Lett. B, 478, 5
[69] Allen, S. W., Schmidt, R. W., Bridle, S. L. 2003b, MNRAS, 346, 596
[70] Cleary, K. 2003, Ph.D thesis, University of Manchester